ELSEVIER

Intermetallics 9 (2001) 799–805

Intermetallics

www.elsevier.com/locate/intermet

Theoretical study on cracking behavior in two-phase alloys $Cr–Cr_2X$ (X = Hf, Nb, Ta, Zr)

Suklyun Hong*, C.L. Fu

Metals and Ceramics Division, Oak Ridge National Laboratory, Oak Ridge, TN 37831-6114, USA

Received 1 February 2001; accepted 10 July 2001

Abstract

To examine the importance of thermal expansion mismatch on cracking in two-phase $Cr–Cr_2X$ (X = Hf, Nb, Ta, Zr) alloys, we have calculated the coefficients of thermal expansion (CTE) of Cr and Laves-phase Cr_2X alloys by local-density-functional approach. A Debye model is used to approximate the phonon contribution through the elastic acoustic response. The sound velocities are determined by the calculated elastic constants and associated anharmonicity. The calculation shows that the CTE of Cr at high temperatures is notably larger than those of Cr_2X. If the difference in CTE between Cr and Cr_2X is a primary source of crack initiation, our results fail to explain the experimental observation that, among these four $Cr–Cr_2X$ alloy systems, the ingot cracking is present mainly in $Cr–Cr_2Nb$. We suggest that for the cracking to occur,the presence of thermal mismatch stresses are retained by a hard and supersaturated Cr matrix (e.g. due to the relatively high solubility of Nb in Cr in the case of $Cr–Cr_2Nb$). On the other hand, the softer Cr matrix can accommodate thermal misfit dislocations plastically even though the CTE difference between Cr and Cr_2X is large. © 2001 Elsevier Science Ltd. All rights reserved.

Keywords: A. Laves phase; B. Elastic properties

1. Introduction

Since single-phase Laves phase alloys are quite brittle, alloy development has been focused on $Cr–Cr_2X$ (X = Hf, Nb, Ta or Zr) two-phase alloy [1–5]. The binary Cr–X phase diagrams [6] show a eutectic reaction, making it possible to produce two-phase alloys of the type $Cr–Cr_2X$. In the two-phase region comprising $Cr–Cr_2X$, eutectic composition results in the occurrence of the phases with a fibrous/rod morphology, and in the hypoeutectic alloys the primary phase is Cr solid solution. At temperatures below the eutectic temperature, the Cr solid solution decomposes to provide secondary Cr_2X precipitates. The Cr phase provides a soft and ductile matrix, resulting in a strong and tough two-phase alloy.

Recently, Kumar and Liu [4] examined the microstructure of a $Cr–Cr_2Nb$ two-phase alloy in the as-cast and annealed conditions using optical and electron microscopy techniques. They found ingot cracking in this system as temperature decreases. Such ingot cracking, however, was not observed in Cr–Hf [3], Cr–Ta [5] and Cr–Zr [5] systems.

In this paper, we investigate if thermal mismatch is a major cause for ingot cracking in these two-phase alloys. To examine the effect of thermal expansion mismatch on cracking, we calculate the coefficients of thermal expansion (CTEs) of Cr and Cr_2X. In Section 2, we outline the theory to calculate the CTE of cubic systems. In Section 3, we present the calculated results which also include the second-order and third-order elastic constants of Cr and Cr_2X. In Section 4, a discussion on the possible cause of ingot cracking is given in terms of the calculated CTEs. This work is summarized in the final section.

2. Theory: thermal expansion coefficient

The coefficient of thermal expansion α for a cubic crystal is given by [7]

$$\alpha = \frac{1}{l}\left(\frac{\partial l}{\partial T}\right)_p = \frac{1}{3V}\left(\frac{\partial V}{\partial T}\right)_p = \frac{1}{3B}\left(\frac{\partial p}{\partial T}\right)_V, \quad (1)$$

where p is the pressure and B is the bulk modulus.

* Corresponding author at present address: Department of Physics, Sejong University, Seoul 143-747, Korea.

E-mail address: hong@sejong.ac.kr (S. Hong).

0966-9795/01/$ - see front matter © 2001 Elsevier Science Ltd. All rights reserved.
PII: S0966-9795(01)00069-3

Nonzero value of CTE results from the anharmonicity of the crystal, i.e. the volume dependence of phonon frequencies. In quasi-harmonic approximation, the free energy F of the crystal is given by

$$F(V, T) = E(V) + F_{\mathrm{ph}}(V, T), \tag{2}$$

$$F_{\mathrm{ph}}(V, T) = k_{\mathrm{B}} T \sum_{ks} \ln\left\{2 \sinh\left(\frac{\hbar\omega_{\mathrm{s}}(k)}{2k_B T}\right)\right\}, \tag{3}$$

where E is the static contribution to the free energy, and F_{ph} is the free energy from phonon modes $\omega_s(k)$. Here, $\omega_{\mathrm{s}}(k)$ is the angular frequency of the normal mode with wave vector **k** in branch s.

From the pressure, we obtain

$$\left(\frac{\partial p}{\partial T}\right)_V = -\frac{\partial^2 F_{\mathrm{ph}}}{\partial V \partial T} = \sum_{ks} \gamma_{ks} c_{vs}(k), \tag{4}$$

where γ_{ks} is the Grüneisen parameter for the normal mode (**k**s) given by

$$\gamma_{ks} = -\frac{\partial(\ln\omega_{\mathrm{s}}(k))}{\partial(\ln V)}, \tag{5}$$

and $c_{vs}(k)$ is the contribution of the mode (**k**s) to the specific heat $c_v = \Sigma_{ks} c_{vs}(k)$.

Since the thermal expansion is dominated by low energy excitations, we use a Debye model to describe the vibrating lattice. In the Debye model, the phonon contribution is approximated through the elastic acoustic response. Since all the normal-mode frequencies scale linearly with the cutoff frequency ω_{D} in the Debye model, we can write

$$\gamma_{ks} \equiv -\frac{\partial(\ln\omega_{\mathrm{D}})}{\partial(\ln V)} = \gamma. \tag{6}$$

Also, within the Debye model, $\left(\frac{\partial p}{\partial T}\right)_V$ is equal to γc_v, so α can be written in a simple form:

$$\alpha = \frac{\gamma c_v}{3B(T)} \tag{7}$$

The temperature dependence of the bulk modulus is obtained from

$$B(T) = V\left(\frac{\partial^2 F}{\partial V^2}\right)_T. \tag{8}$$

Using the relation $k_B \Theta_{\mathrm{D}} = \hbar\omega_{\mathrm{D}}$, Eq. (6) becomes

$$\gamma = -\frac{\partial(\ln\Theta_{\mathrm{D}})}{\partial(\ln V)} = -\frac{V}{\Theta_{\mathrm{D}}}\frac{\partial\Theta_{\mathrm{D}}}{\partial V}, \tag{9}$$

where the Debye temperature Θ_{D} is given by

$$\Theta_{\mathrm{D}} = \frac{\hbar}{k_B}\left(\frac{6\pi^2 N}{V}\right)^{1/3} v_{\mathrm{m}} \tag{10}$$

Here, v_{m} denotes the mean sound velocity of the propagation of elastic waves in the continuum. The propagation velocities v_is are the solutions of the cubic equation (Christoffel equation) in v^2 [8,9]:

$$\left|\Gamma_{ik} - \delta_{ik}\rho v^2\right| = 0 \tag{11}$$

where Γ_{ik} ($i,k = 1,2,3$) are the Christoffel stiffnesses, subject to the condition $\Gamma_{ik} = \Gamma_{ki}$. For cubic systems, if a_1, a_2, a_3 are the direction cosines of the normal to the wave front, the six Christoffel stiffnesses are given in terms of three independent elastic constants C_{11}, C_{12}, C_{44}:

$$\Gamma_{11} = C_{11}a_1^2 + C_{44}\left(a_2^2 + a_3^2\right) \tag{12}$$

$$\Gamma_{12} = (C_{12} + C_{44})a_1 a_2 \tag{13}$$

$$\Gamma_{13} = (C_{12} + C_{44})a_1 a_3 \tag{14}$$

$$\Gamma_{22} = C_{11}a_2^2 + C_{44}\left(a_1^2 + a_3^2\right) \tag{15}$$

$$\Gamma_{23} = (C_{12} + C_{44})a_2 a_3 \tag{16}$$

$$\Gamma_{22} = C_{11}a_3^2 + C_{44}\left(a_1^2 + a_2^2\right) \tag{17}$$

Therefore, the information of elastic constants at several volumes enables us to determine Debye temperature, Grüneisen parameter, bulk modulus, and thus the coefficient of thermal expansion.

3. Results

3.1. Elastic constants

We performed total-energy calculations using the full-potential linearized augmented plane-wave (FLAPW) method within the local-density approximation. The FLAPW method solves the local-density-functional equations without any shape approximation to the potential or charge density. The atomic positions are relaxed by calculating Hellmann–Feynman forces acting on the atoms.

First, we obtained the theoretical equilibrium lattice constants. For bcc Cr, a lattice constant of 2.79 Å was obtained which is in fair agreement with the experimental value of 2.88 Å. The theoretical lattice constants of Laves phases Cr_2X are 6.947 Å (X = Hf), 6.822 Å (X = Nb), 6.809 Å (X = Ta), and 6.990 Å (X = Zr), which are smaller than the experimental lattice constants 7.157

[10], 6.991 [2], 6.985 [4], 7.208 [10] Å, respectively, by 2–3%.

To determine the Debye temperatures, we evaluated the elastic constants (and from which the sound velocities are obtained by averaging over at least 100 directions). Under elastic strains, the new orthogonal lattice axes a_i' are related to the original ones a_j by $a_i' = (1+\varepsilon_{ij})a_j$, where $i,j = x, y, z$ and

$$\varepsilon_{ij} = \begin{pmatrix} e_1 & e_6/2 & e_5/2 \\ e_6/2 & e_2 & e_4/2 \\ e_5/2 & e_4/2 & e_3 \end{pmatrix} \tag{18}$$

is the strain tensor, and e_is are the strain components. The elastic strain energy density U is given by

$$U = \frac{1}{2}\sum_{i=1}^{6}\sum_{j=1}^{6}\widetilde{C}_{ij}e_ie_j, \tag{19}$$

where $C_{ij} = \frac{1}{2}\left(\widetilde{C}_{ij} + \widetilde{C}_{ji}\right)$ and C_{ij}s are the elastic constants. The cubic structure has only three independent elastic constants C_{11}, C_{12}, and C_{44}. These elastic constants were determined from three relations (i) $U = (C_{11}-C_{12})\,e^2$ for $e_1 = -e_2 \equiv e$, (ii) $U = (C_{11}+C_{12})e^2$ for $e_1 = e_2 = e$,and (iii) $U = \frac{1}{2}C_{44}e^2$ for $e_6 = e$, where the unspecified strain components are zero for each of these cases. The total energy was calculated as a function of strains (up to 3–4%) for each of these deformation. The elastic constants are then obtained from the curvature of total energy-strain curves by fitting the calculated values to third-order polynomials [11].

The second-order elastic constants were calculated at three different lattice constants in the vicinity of the experimental lattice constant. The volume dependence of these second-order elastic constants gives rise to the higher-order elastic constants. The results of elastic constants at experimental volume for Cr and Cr_2X are given in Table 1.

Note that bulk Cr displays a long-wavelength spin-density wave with a short-range antiferromagnetic ordering below the Néel temperature of $T_N = 311$ K. Therefore, we calculated the elastic constants of Cr for both antiferromagnetic and paramagnetic cases. The calculated values of antiferromagnetic Cr in Table 1 should be compared with the experimental elastic constants $C_{11} = 391$, $C_{12} = 89.6$, and $C_{44} = 103$ GPa of Cr measured at 77 K [12].

For Cr_2X, no single crystal data are available. However, the Hill's averages [8] of Young's and shear moduli of Cr_2X always give smaller values than those of experimental measurements [14]. An independent calculation by Ormeci et al. [15] for Cr_2Nb also showed a similar trend as found in our result. The reasons for this discrepancy remain unclear. (The calculated elastic constants at the theoretical lattice parameter should be higher than the measured values, since the theoretical lattice parameters are usually 2–3% smaller than the experimental lattic parameters. The present calculations, however, show opposite trend). The calculated elastic constants at different volumes are shown in Figs. 1 and 2. As expected, the elastic constants increase with increasing unit cell volume. Furthermore, all the calculated elastic constants of Cr and Cr_2X show a linear dependence on volume within the volume range we have considered, which indicates that third-order elastic constants are dominant in the elastic anharmonicity.

By writing the third-order contribution to the elastic energy density U as

$$U^{(3)} = \frac{1}{3!}\sum_{\mu\nu\sigma} C_{\mu\nu\sigma}e_\mu e_\nu e_\sigma, \tag{20}$$

the slopes of lines shown in Figs. 1 and 2 are related to the third-order elastic constants through the following expressions:

$$C_{11} = (C_{11})_0 + \frac{1}{3}(C_{111} + 2C_{112})\frac{\delta V}{V}, \tag{21}$$

$$C_{12} = (C_{12})_0 + \frac{1}{3}(C_{123} + 2C_{112})\frac{\delta V}{V}, \tag{22}$$

$$C_{44} = (C_{44})_0 + \frac{1}{3}(C_{144} + 2C_{166})\frac{\delta V}{V}, \tag{23}$$

where $(C_{11})_0$, $(C_{12})_0$ and $(C_{44})_0$ are second-order elastic constants at a reference volume, e.g. the experimental volume. Since so far we have considered only three independent deformations, the slopes of lines shown in Figs. 1 and 2 can only give the linear combinations of $C_{111} + 2C_{112}$ and $C_{123} + 2C_{112}$, and $C_{144} + 2C_{166}$. These values are tabulated in Table 2, where the negative values are due to the fact that the elastic constants decrease linearly with increasing lattice parameter. To obtain the third-order elastic constants individually, independent deformations are required. This can be achieved, for example, by setting $e_1 = e$ as the only non-zero strain component in Eq. (18). We then have

Table 1
Calculated elastic constants (in units of GPa) at experimental volumes for Cr and Cr_2X (X = Hf, Nb, Ta, Zr)[a]

	C_{11}	C_{12}	C_{44}
Cr (antiferro)	373 (391, 350)	65 (89.6, 57.8)	81 (103, 101)
Cr (para)	393	122	68
Cr_2Hf	225	126	58
Cr_2Nb	250	170	58
Cr_2Ta	281	173	73
Cr_2Zr	201	126	46

[a] The two numbers in each parenthesis for Cr (antiferro) are the experimental value obtained at low temperature of 77 K [12] and that from Ref. [13], respectively.

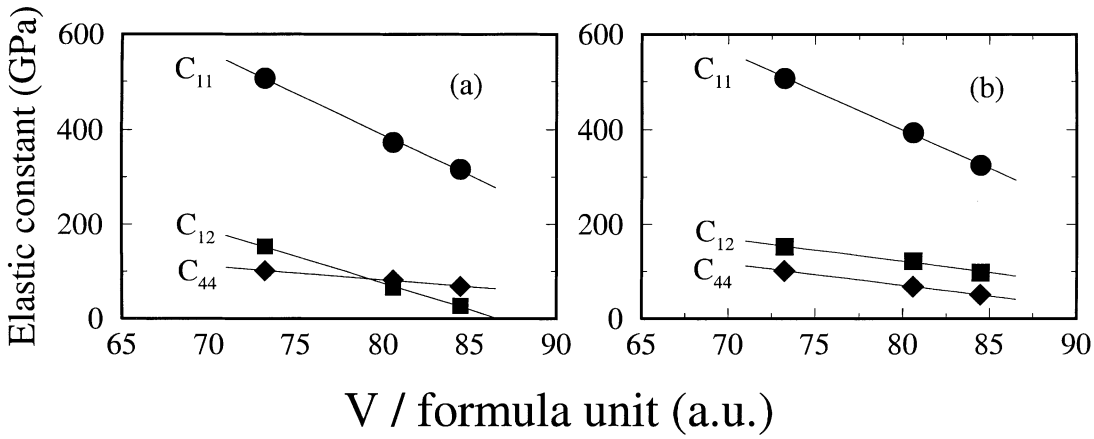

Fig. 1. Calculated elastic constants (in units of GPa) at all three volumes mentioned in text for (a) antiferromagnetic and (b) paramagnetic Cr. Each line is a linear fit of three data points of C_{11} (circle), C_{12} (square), and C_{44} (diamond).

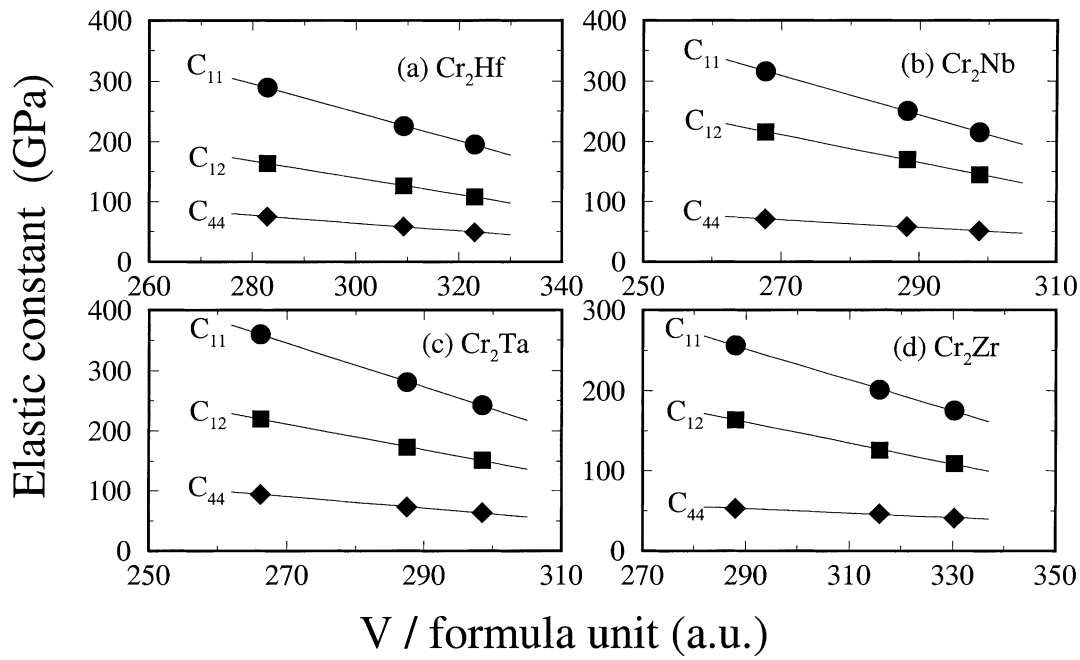

Fig. 2. Calculated elastic constants (in units of GPa) at all three volumes mentioned in text for (a) Cr_2Hf, (b) Cr_2Nb, (c) Cr_2Ta, and (d) Cr_2Zr. Each line is a linear fit of three data points of C_{11} (circle), C_{12} (square), and C_{44} (diamond).

$$C_{11} = (C_{11})_0 + C_{111}e. \tag{24}$$

For the present purpose, however, the combinations of third-order terms are sufficient for our discussion.

We note that, among these Cr_2X compounds, the magnitudes of the third-order elastic constants are the lowest for Cr_2Zr, indicating a low CTE value for this compound (see next section).

3.2. Coefficient of thermal expansion

The solutions of the Christoffel equation give rise to the mean sound velocity, from which the Debye temperature is obtained. Since Θ_D scales linearly with volume, which is confirmed with a direct calculation, we approximate $\frac{\partial\Theta_D}{\partial V} \approx \frac{\Delta\Theta_D}{\Delta V}$. This enables us to obtain γ at given volumes with $\gamma \approx -\frac{V}{\Theta_D}\frac{\Delta\Theta_D}{\Delta V}$. The mean sound velocity v_m, Debye temperature Θ_D, Grüneisen parameter γ, Bulk modulus B_0, and the CTE at high temperatures (e.g. 1000 K) α^* are given for Cr and Cr_2X at their experimental volumes in Tables 3 and 4 .

The CTE as a function of temperature is shown in Fig. 3. The discontinuity of CTE for Cr shown in Fig. 3 is due to the magnetic phase transition at Néel temperature of 311 K, below which Cr has antiferromagnetic ordering and above which Cr becomes paramagnetic. In this calculation, the magnetic entropy due to the magnetic fluctuations is not included. Even without the

Table 2
Calculated third-order elastic constants (in units of GPa) for Cr and Cr_2X (X = Hf, Nb, Ta, Zr)

	$(C_{111}+2C_{112})/3$	$(C_{123}+2C_{112})/3$	$(C_{144}+2C_{166})/3$
Cr (antiferro)	−1372	−905	−237
Cr (para)	−1315	−395	−366
Cr_2Hf	−724	−431	−200
Cr_2Nb	−938	−661	−186
Cr_2Ta	−1052	−615	−276
Cr_2Zr	−605	−411	−90

Table 3
Calculated thermoelastic quantities of Cr at experimental volume: the mean sound velocity (v_m), the Debye temperature (Θ_D), the Grüneisen parameter (γ), the bulk modulus (B); the coefficient of thermal expansion at 1000 K is denoted as α^*

	v_m (m/s)	Θ_D (K)	γ	B (GPa)	α^* (10^{-6}/K)
Cr (af)	4186	545	1.10	168	–
Cr (para)	3907	509	2.02	212	12.26

Table 4
Calculated thermoelastic quantities of Cr_2X (X = Hf, Nb, Ta, Zr) at their experimental volumes

	v_m (m/s)	Θ_D (K)	γ	B (GPa)	α^* (10^{-6}/K)
Cr_2Hf	2590	311	1.39	159	8.53
Cr_2Nb	2881	354	1.44	197	7.66
Cr_2Ta	2713	334	1.70	209	8.59
Cr_2Zr	2788	332	0.91	151	5.56

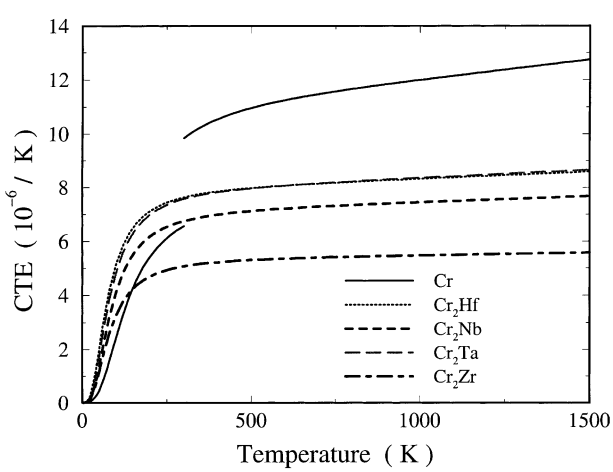

Fig. 3. The calculated coefficient of thermal expansion of Cr and Cr_2X (X = Hf, Nb, Ta, Zr) as a function of temperature. Note discontinuity of Cr due to the phase transitionat Neel temperature (311 K).

magnetic entropy, the CTE of Cr gives a very good agreement with experimental measurements at low temperatures (< 200 K) and at high temperatures [16]. Since we focus on the high-temperature behaviors in this paper, a further investigation on the effect of magnetic entropy around Néel temperature will be considered elsewhere.

For Cr_2X alloys, we found that: (i) the CTE of Cr at high temperatures is notably larger than those of Cr_2X; in particular, the CTE of Cr is about twice of that of Cr_2Zr, and (ii) the CTEs of Cr_2Hf and Cr_2Ta are nearly equal and are very close with that of Cr_2Nb.

An estimation of CTE from experimental data [4,17] of Cr and Cr_2Nb gives $11–12\times10^{-6}$/K and $\sim8\times10^{-6}$/K around 1000 K, respectively. For both Cr and Cr_2Nb, we found a good agreement between theory and experiment at high temperatures [see Fig. 4(a) for Cr_2Nb]. Experimentally [18], the CTE of Cr_2Ta is $6–10\times10^{-6}$/K in going from 300 K to 1500 K. Fig. 4(b) shows the comparison between theory and experiment for Cr_2Ta. The theoretical CTE agrees reasonably well with experiment in magnitude.

4. Discussion

Now, we can discuss if thermal mismatch is a major cause for ingot cracking in these Laves two-phase alloys by examining the difference in CTE between Cr and Cr_2X. As mentioned already, among these Cr-based two phase alloys Cr–Cr_2X (X = Hf, Nb, Ta, Zr), the ingot cracking is present mainly in Cr–Cr_2Nb system. If the difference in CTE between Cr and Cr_2X is a primary measure on the occurrence of crack, our results fail to explain the experimental observation. This is because the CTE of Cr is notably larger than those of Cr_2X considered here, in particular than that of Cr_2Zr. Thus, we suggest that the mismatch due to the difference in CTEs is not a major source for ingot cracking in these two-phase alloys; other sources may play important roles in crack initiation.

It was suggested by Kumar and Liu [4], that the presence of appreciable (~6 at.%) Nb solubility in the Cr matrix at the eutectic temperature and the difficulty in precipitating the Nb out as Cr_2Nb during cooling can be a source contributing to the cracking. (For the measured solubility of X in the Cr matrix, see Table 5.) In contrast, for Cr–Hf system, there is negligible Hf solubility in the Cr matrix at the eutectic temperature and so matrix supersaturation is not evident, which would render the matrix softer and more tolerant to cracking. Similarly, this is also the case for Cr–Zr system since the Zr solubility in the Cr matrix is negligible (< 0.6%). For the Cr–Ta system, there is a small amount of Ta solubility in the Cr matrix at the eutectic temperature and so matrix supersaturation, if any, will be less dominant than in the Cr–Nb system. On the other hand, the CTE of Cr_2Ta is closer to that of Cr than Cr_2Nb and Cr_2Zr.

In addition to the solid solution hardening contributing to cracking in the case of Cr–Nb system, the presence of appreciable second element in solid solution may also

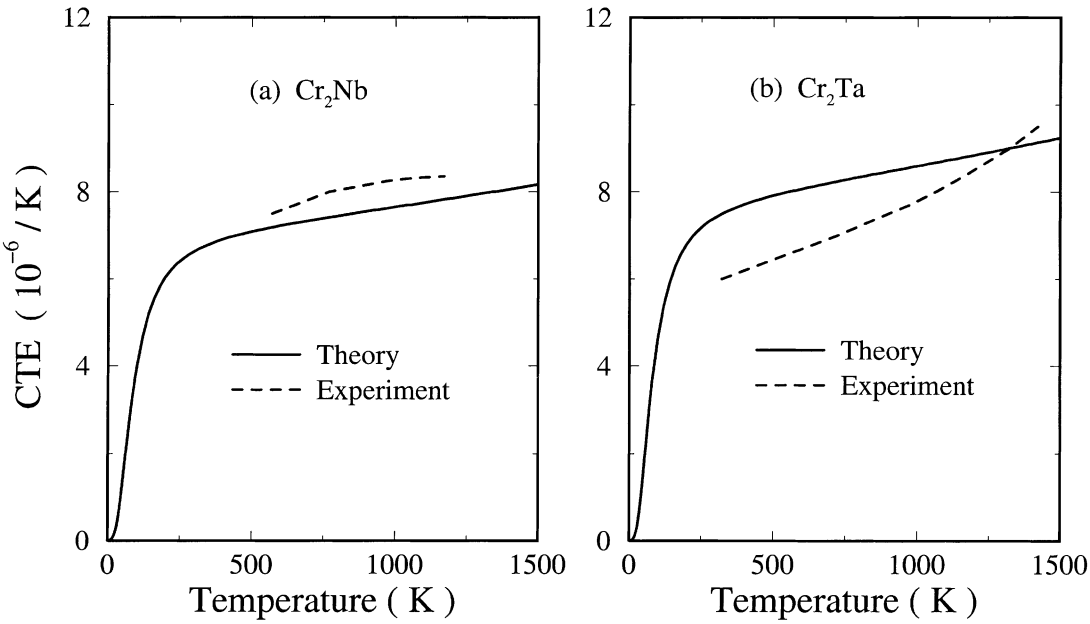

Fig. 4. The coefficient of thermal expansion of (a) Cr_2Nb and (b) Cr_2Ta as a function of temperature. Theoretical results are compared with experiment.

Table 5
The maximum solubility of X (= Hf, Nb, Ta, Zr) in the Cr solid-solution matrix from the binary Cr–X phase diagrams [6]

X	Maximum solubility (at.% of X)
Hf	Negligible
Nb	~6
Ta	~4
Zr	< 0.6

increase the ductile/brittle transition temperature of the matrix Cr. Thus, due to the presence of Nb, there is not only a decrease in ductility of the Cr matrix but also a larger temperature range over which it has to accommodate the mismatch in a brittle state.

Thus, we suggest that for the crack to occur, the presence of thermal mismatch stresses are retained by a hard and supersaturated Cr matrix (e.g. in the case of Cr–Cr_2Nb). On the other hand, a soft Cr matrix can accommodate thermal misfit dislocations plastically even though the CTE difference between Cr and Cr_2X is large (e.g. in the case of Cr–Cr_2Zr and Cr–Cr_2Hf).

5. Summary

The thermoelastic properties of Cr and Laves phases Cr_2X (X = Hf, Nb, Ta, Zr) alloys were presented. The calculated results were used to explain the experimental observation that the ingot cracking occurs mainly in the Cr–Cr_2Nb two-phase alloy sytem. The calculated CTEs are in reasonably good agreement with available experiments for Cr_2Nb and Cr_2Ta. We also found that the CTE of Cr is much higher than those of Cr_2X. Therefore, if the difference in CTE between Cr and Cr_2X is a primary source of crack initiation, our results failed to explain the experimental fact that, among these Cr–Cr_2X alloys, the ingot cracking is present mainly in Cr–Cr_2Nb. We suggested that, for the cracks to occur, the presence of thermal mismatch stresses are retained by a hard and supersaturated Cr matrix as in the case of Cr–Cr_2Nb. On the other hand, the softer Cr matrix can accommodate thermal misfit dislocations plastically even though the CTE difference between Cr and Cr_2X is large.

Acknowledgements

We acknowledge C.T. Liu and D.J. Thoma for providing unpublished results on CTE of Cr_2Nb and Cr_2Ta. Also, helpful discussions with C.T. Liu are greatly appreciated. The work was sponsored by the Division of Materials Sciences and Engineering, Office of Basic Energy Sciences. Oak Ridge National Laboratory is operated by UT-Battelle, LLC, for the US Department of Energy under contract DE-AC05-00OR22725.

References

[1] Takeyama M, Liu CT. Mater Sci Eng 1991;A 132:61.
[2] Thoma DJ, Perepezko JH. Mater Sci Eng 1992;A 156:97.
[3] Kumar KS, Miracle DB. Intermetallics 1994;2:257.
[4] Kumar KS, Liu CT. Acta Mater 1997;45:3671.
[5] Liu CT. Unpublished.

[6] Massalski TB, editor, Binary alloy phase diagram, vol. 1. Metals Park OH: ASM, 1986 (For more recent phase diagram of Cr_2Nb, see Ref. [2]).
[7] Ashcroft NW, Mermin ND. Solid state physics. Holt, Rinehart and Winston, 1976. p. 487–509.
[8] Hearmon RFS. An introduction to applied anisotropic elasticity. London: Oxford University Press, 1961, p. 68–89.
[9] Ashcroft NW, Mermin ND. Solid state physics. Holt, Rinehart and Winston, 1976, p. 443–7.
[10] Villars P, Calvert LD. Pearson's handbook of crystallographic data for intermetallic phases, vol. 2. Metals Park, OH: ASM, 1985. p. 1908.
[11] Hong S, Fu CL. Intermetallics 1999;7:5.
[12] Bolef DI, de Klerk J. Phys Rev 1963;129:1063.
[13] Hirth JP, Lothe J. Theory of dislocations. 2nd ed. New York: Wiley, 1982.
[14] Chu F. Private communication.
[15] Ormeci A, Chu F, Wills JM, Chen SP, Albers RC,Thoma DJ, Mitchell TE, et al. In: High-temperature ordered intermetallic alloys VII. MRS Symp Proc 1996; 460: 623.
[16] White GK, Roberts RB, Fawcett E. J Phys F: Met Phys 1986; 16:449.
[17] Thoma DJ. Unpublished.
[18] Liu CT. Unpublished.